Available online at www.sciencedirect.com

SciVerse ScienceDirect

Scripta Materialia 68 (2013) 380–383

Scripta MATERIALIA

www.elsevier.com/locate/scriptamat

Viewpoint Paper

A novel high-strength, high-ductility and high-corrosion-resistance FeAlMnC low-density alloy

Po-Chih Chen, Chuen-Guang Chao and Tzeng-Feng Liu*

Department of Materials Science and Engineering, National Chiao Tung University, Hsinchu, Taiwan, ROC

Available online 26 October 2012

Abstract—The as-quenched Fe–8.68 wt.% Al–30.5 wt.% Mn–1.85 wt.% C alloy is plasma-nitrided at 500 °C for 8 h. The nitrided layer obtained is 40 μm thick and composed predominantly of AlN, with a small amount of Fe_4N. The resultant surface hardness (1860 Hv), substrate hardness (550 Hv), ductility (33.6%) and corrosion resistance in 3.5% NaCl solution in the present nitrided alloy are far superior to those obtained previously in optimally nitrided high-strength alloy steels, as well as martensitic and precipitation-hardening stainless steels.

Keywords: Spinodal decomposition; Plasma nitriding; Corrrosion resistance; Microhardness; FeAlMnC alloy

Introduction

The austenitic Fe–Al–Mn–C quarternary alloys have been attracting tremendous attention because of their excellent combinations of high strength and high ductility and because they have no need for expensive strategic alloying elements (e.g. Cr, Ni, Mo). Moreover, due to the high aluminum content, the density of the alloys is ~13% lower than conventional steels [1]. Previous studies have shown that the as-quenched microstructure of Fe–(7.8–10) wt.% Al–(28–30) wt.% Mn–(0.8–1.3) wt.% C alloys was single-phase austenite (γ) [1–5]. An optimal combination of strength and ductility could be obtained for the Fe–Al–Mn–C alloys aged at 550 °C for ~16 h [2,3]. Under these aging conditions, a high density of fine $(Fe,Mn)_3AlC$ carbides (κ′-carbides) having an $L'1_2$ (ordered face-centered cubic, fcc) structure precipitated coherently within γ matrix without any grain boundary precipitates. After optimal aging, the ultimate tensile strength (UTS), yield strength (YS) and elongation (El) of the Fe–Al–Mn–C alloys could reach 1130–1250 MPa, 1080–1120 MPa and 33–31%, respectively [2,3].

Recently, we investigated the as-quenched microstructure of the Fe–9.8 wt.% Al–29 wt.% Mn–(1.45–2.05) wt.% C alloys, and found that an extremely high density of nano-sized κ′-carbides was formed within γ matrix by spinodal decomposition during quenching [6]. This is quite different from that observed in the austenitic Fe–Al–Mn–C ($C \leqslant 1.3$ wt.%) alloys, in which fine κ′-carbides could only be observed in aged alloys. Due to the pre-existing nano-sized κ′-carbides, the aging temperature and time required to attain the optimal combination of strength and ductility are, respectively, much lower and less than those of the previous Fe–Al–Mn–C ($C \leqslant 1.3$ wt.%) alloys. For example, with almost equivalent elongation, the Fe–9 wt.% Al–28 wt.% Mn–1.8 wt.% C alloy aged at 450 °C for 12 h can possess yield strength ~28% higher than that of the optimally aged Fe–Al–Mn–C ($C \leqslant 1.3$ wt.%) alloys [7].

Although the austenitic Fe–Al–Mn–C alloys could possess excellent combinations of strength and ductility, the corrosion resistance of the alloys was insufficient for applications in aggressive environments [4,5]. Plasma nitriding was widely utilized to improve surface hardness and corrosion resistance of metallic materials [8–19]. However, to date, little information concerning the plasma nitriding treatment for Fe–Al–Mn–C alloys has been reported in the literature. The main purpose of this work is to investigate the characteristics of an Fe–8.68 wt.% Al–30.5 wt.% Mn–1.85 wt.% C alloy after plasma nitriding at 500 °C for 8 h.

The Fe–8.68 wt.% Al–30.5 wt.% Mn–1.85 wt.% C alloy was prepared in an air induction furnace. After being homogenized at 1150 °C for 6 h, the ingot was hot-rolled to a 6 mm thick plate. The plate was subsequently solution heat-treated at 1200 °C for 2 h and then quenched

* Corresponding author. Tel.: +886 3 5131288; fax: +886 3 5713987; e-mail: tfliu@cc.nctu.edu.tw

1359-6462/$ - see front matter © 2012 Acta Materialia Inc. Published by Elsevier Ltd. All rights reserved.
http://dx.doi.org/10.1016/j.scriptamat.2012.10.034

into room-temperature water. The specimen was polished using SiC papers to 2400 grit before plasma nitriding. The plasma nitriding process was performed at 500 °C for 8 h using an atmosphere of 50% N_2 and 50% H_2 under a pressure of 130 Pa. X-ray diffraction (XRD) was carried out using a Bruker D8 with Cu-K_α radiation. The nitrogen concentration and microhardness of the nitrided alloy were determined by using glow discharge spectrometer (GDS) and Vicker's indenter at 100 gf, respectively. Potentiodynamic polarization curves were measured in 3.5% NaCl solution at 25 °C with a scan rate of 2 mV s^{-1}. A saturated calomel electrode (SCE) and a platinum wire were used as reference and auxiliary electrodes, respectively. Tensile tests were carried out at room temperature with an Instron 8501 tensile testing machine at a strain rate of 6.7×10^{-4} s^{-1}.

Figure 1a is a transmission electron microscopy (TEM) $(100)_{\kappa'}$ dark-field image and the corresponding diffraction pattern of the as-quenched alloy, revealing that an extremely high density of nano-sized κ′-carbides can be observed within γ matrix and the nano-sized κ′-carbides were formed by spinodal decomposition during quenching [6,7]. By using a LECO 2000 image analyzer, the average size and volume fraction of the κ′-carbides were determined to be ~10 nm and 38%, respectively. A detailed investigation indicated that when the as-quenched alloy was aged at 500 °C for 8 h, the alloy could possess an excellent combination of strength and ductility with the UTS, YS and El being 1402 MPa, 1298 MPa and 34.5%, respectively. For achieving the effects of aging and nitriding simultaneously, the plasma nitriding was fixed at 500 °C for 8 h with various processing pressures and gas compositions. The experiments indicated that the working pressure of 130 Pa with a gas composition of 50% N_2 and 50% H_2 could give rise to the best plasma nitriding results. Figure 1b is a cross-sectional scanning electron microscopy (SEM) image of the nitrided alloy, showing that the thickness of the nitrided layer is ~40 μm. The grain boundaries of the substrate are clearly revealed by the nital etchant, while the nitrided layer remains intact. Moreover, the boundary between nitrided layer and substrate is obscure. Figure 1c shows the XRD result for the nitrided alloy, revealing that besides γ diffraction peaks, diffraction peaks belonging to AlN and Fe_4N can also be detected. Both AlN and Fe_4N have an fcc structure with lattice parameters of 4.06 nm and 3.79 nm, respectively [20,21]. Moreover, the intensity of the AlN diffraction peaks is much higher than that of Fe_4N phase, indicating that the nitrided layer is composed predominantly of AlN phase with a significantly less amount of Fe_4N phase. Furthermore, the XRD peaks are fairly broadened, which may be due to the large amount of nitrogen incorporated in these phases [11–12,15–19]. Figure 2a shows the nitrogen concentration as a function of depth, revealing that at the outmost surface, the nitrogen concentration is as high as ~20 wt.% (48 at.%). The nitrogen concentration gradually decreases with increasing depth. Figure 2b shows the microhardness of the nitrided alloy as a function of depth. The surface microhardness is extremely high (1860 Hv), and gradually decreases with increasing depth until the substrate value is ~550 Hv. Tensile test indicated that UTS, YS and El of the nitrided alloy were 1388 MPa, 1286 MPa and 33.6%, respectively, which are comparable to those obtained for the same alloy aged at 500 °C for 8 h. By slightly tilting the specimen, the fracture and free surfaces could be observed simultaneously, as illustrated in Figure 2c. High density of dimples can be seen within the austenite + κ′-carbides matrix, and no microvoids or microcracks are observed in the vicinity of the interface between nitrided layer and substrate. Obviously, the substrate remains ductile and the nitrided layer itself is very compact with good adhesion to the substrate.

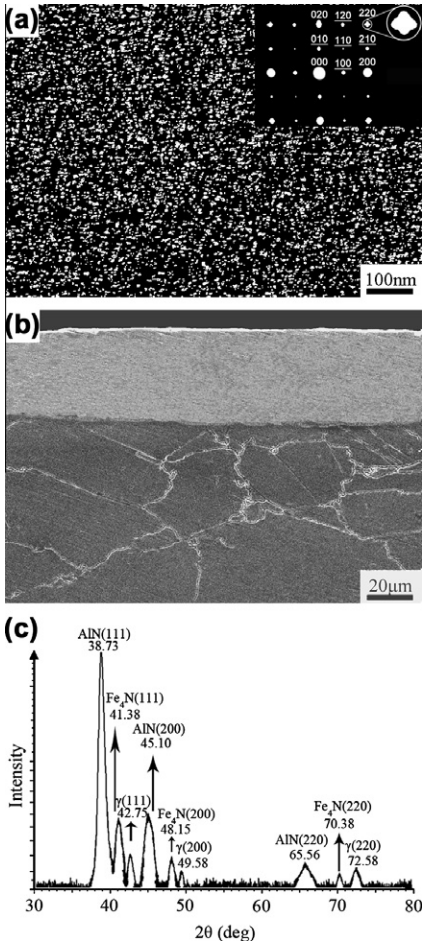

Figure 1. (a) TEM $(100)_{\kappa'}$ dark-field image and corresponding diffraction pattern (hkl: γ, hkl: κ′-carbide) of the as-quenched alloy. (b) SEM image of the present nitrided alloy (etched in 5% nital). (c) X-ray diffraction pattern for the present nitrided alloy.

Potentiodynamic polarization curves for as-quenched and plasma nitrided alloys in 3.5% NaCl solution are shown in Figure 3a. Evidently, for the untreated alloy (curve I), there is no apparent passivation region. The corrosion current density (i_{corr}) and corrosion potential (E_{corr}) are 2×10^{-6} A cm^{-2} and −790 mV, respectively. However, an obvious passivation region can be observed for the nitrided alloy (curve II), and i_{corr} is evidently reduced by about three orders of magnitude to 6×10^{-10} A cm^{-2} and E_{corr} is drastically improved to +50 mV. Moreover, the values of the pitting corrosion current density (i_p) and pitting potential (E_{pit}) for the nitrided alloy are 2×10^{-7} A cm^{-2} and +2030 mV, respectively. Apparently, plasma nitriding has resulted in a pronounced enhancement in corrosion resistance. Figure

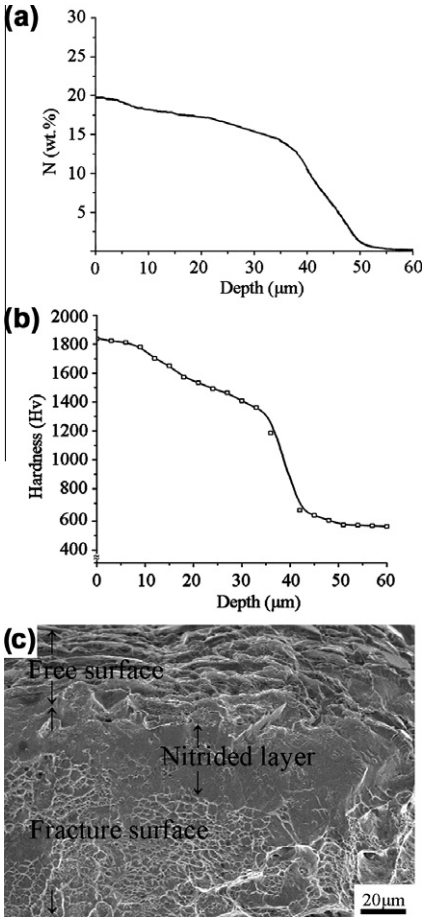

Figure 2. (a) Nitrogen concentration profile measured by GDS of the present nitrided alloy. (b) Hardness profile of the present nitrided alloy. (c) SEM image of the present nitrided alloy after tensile test.

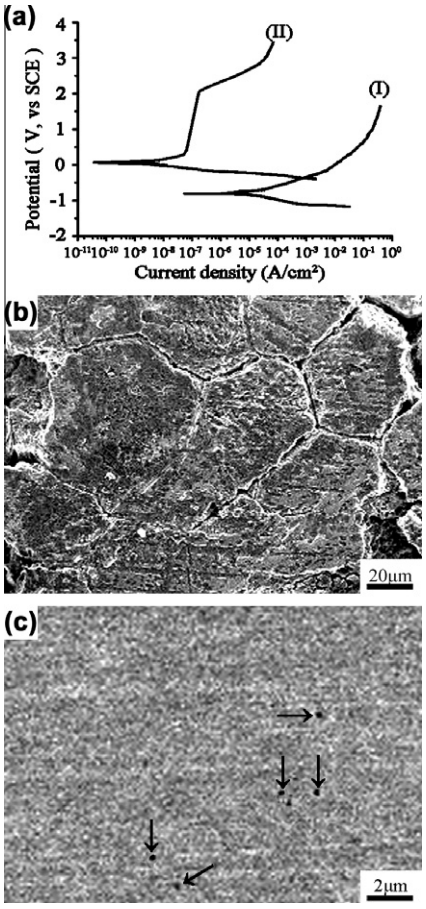

Figure 3. (a) Polarization curves for the present untreated and nitrided alloys in 3.5% NaCl solution. (b) and (c) SEM images of the corroded surfaces for the present untreated and nitrided alloys, respectively.

3b and c shows SEM images of the corroded surfaces, indicating that during polarization the grain boundaries and γ matrix of the untreated alloy were severely attacked, while only a few very small (~0.3 μm) corrosion pits (as indicated with arrows in Fig. 3c) were formed for the nitrided alloy.

That the nitrided layer of the present nitrided alloy is composed predominantly AlN with a small amount of Fe_4N is a remarkable feature. For many industrial applications requiring high strength, high wear resistance and high corrosion resistance, the nitrided low-Cr (Cr < 1.2 wt.%) alloy steels (e.g. AISI 4140, 4340 and 5140) and high-Cr (Cr > 12 wt.%) martensitic stainless steels (e.g. AISI 410) as well as precipitation-hardening (PH) stainless steels (e.g. AISI 17-4PH) were widely used. According to extensive previous studies, the optimal nitriding conditions for the low-Cr steels were 520–550 °C for 4–6 h [8–10], while those for high-Cr stainless steels were 400–480 °C for 2–20 h [11–19]. The nitrided layer formed in these body-centered cubic (bcc) steels is mainly composed of Fe_3N (hexagonal close packed, hcp) and Fe_4N (fcc), without or with a trace of CrN (fcc) [8–19]. After optimal nitriding treatment, the surface microhardness of the low-Cr alloy steels and high-Cr stainless steels were between 890–940 Hv and 1000–1350 Hv, respectively, which are far lower than 1860 Hv obtained in the present nitrided alloy. The primary reason is that due to AlN formation in the present nitrided alloy, nitrogen concentration near the surface can reach 20 wt.%, whereas the surface nitrogen concentrations of the optimally nitrided low-Cr alloy steels and high-Cr stainless steels were 5.7–10 wt.% and 10–15 wt.%, respectively [17,22–25]. The hardness of the nitrides generally increases with increasing nitrogen concentration. For instance, the hardness of AlN is 25.7 GPa [26], which is much higher than that of Fe_3N (11.2–12.4 GPa), and Fe_4N (8.6–11.2 GPa) [22,27]. It is worthwhile to emphasize here that the substrate hardness (550 Hv) of the present nitrided alloy is also much higher than 210–400 Hv obtained in the optimally nitrided high-strength alloy steels and stainless steels [9–16,18]. The reason is that prior to nitriding, these steels need to temper at 15 °C above the nitriding temperature [28], and then nitrided at the optimal temperature for a long duration. This would deteriorate the substrate hardness drastically [23]. Detailed comparisons of surface hardness and substrate hardness are listed in Table 1.

The most important indicators for evaluating the corrosion resistance of metallic materials are i_{corr}, i_p, E_{corr} and E_{pit}; lower current densities and higher potentials indicate better corrosion resistance [8–19]. Table 1 lists the values of i_{corr}, i_p, E_{corr} and E_{pit} obtained using the same SCE in 3.5% NaCl solution at room temperature for the present nitrided alloy, and the previous results for the optimally nitrided low-Cr alloy steels (including

Table 1. Comparisons of polarization test results in 3.5% NaCl solution and hardness of the present nitrided alloy and the optimally nitrided alloy steels as well as various stainless steels.

Alloy	Polarization test results in 3.5% NaCl solution					Hardness (Hv)	
	I_{corr} (A/cm^2)	I_p (A/cm^2)	E_{corr} (mV)	E_{pit} (mV)	ΔE (mV)	Surface	Substrate
Alloy steels	8×10^{-8}~4×10^{-7}	4×10^{-6}~9×10^{-6}	−400~−200	+500~+800	+770~+1000	890~940	275~320
410 (MSS)	6×10^{-8}~6×10^{-7}	8×10^{-5}~8×10^{-4}	−220~−30	+50~+600	+270~+630	1150~1204	210~262
17-4PH(SS)	4.1×10^{-6}~9×10^{-6}	9×10^{-6}~1.3×10^{-5}	−208~−207	+700~+715	+907~+923	1160~1167	360~400
304 (SS)	1.46×10^{-8}~1×10^{-7}	4×10^{-7}~2×10^{-6}	−300~−98	+125~+400	+425~+498	1000~1200	220~250
316 (SS)	1×10^{-7}~3.5×10^{-7}	1×10^{-5}~8×10^{-5}	−330~−83.8	+600~+1200	+683.8~+1330	1350	220
Present alloy	6×10^{-10}	2×10^{-7}	+50	+2030	+1980	1860	550

4140, 4340 and 5140), 410 martensitic stainless steels and 17-4PH stainless steels. For comparison, the results for optimally plasma nitrided lower-strength austenitic stainless steels (AISI 304 and 316) are also listed in Table 1. Evidently, under the same testing conditions, the i_{corr} and i_p of the present alloy are two or three orders of magnitude lower, while the values of E_{corr} and E_{pit} are significantly higher than those of the alloy steels and stainless steels, indicating that the present nitrided alloy has far superior corrosion resistance in 3.5% NaCl solution. Moreover, the size of the surface corrosion pits of the present nitrided alloy is only about 0.3 μm (Fig. 3c), which is much smaller than that (10–200 μm) observed in optimally nitrided alloy steels and stainless steels under similar polarization tests [8–9,12–14]. The lower i_p value results in smaller corrosion pits [12,14], which is in good agreement with the experimental results shown in Table 1. Another important criterion for evaluating the pitting resistance is the difference between E_{pit} and E_{corr}, namely $\Delta E = E_{pit} - E_{corr}$ [29]. In Table 1, the ΔE value for optimally nitrided alloy steels and stainless steels is between +270 and +1330 mV, while that for the present nitrided alloy is +1980 mV, which again demonstrates the superior characteristics of the present nitrided alloy, presumably due to the high nitrogen concentration at surface [17].

Another feature of the present study is that after etching the boundary between nitrided layer and substrate was obscure (Fig. 1b) and no microvoids or cracks could be detected between the nitrided layer and substrate of the fractured surface (Fig. 2c). This is attributed to the fact that both AlN and Fe_4N phases have the same fcc crystal structure as the γ matrix and κ′-carbides with very similar lattice parameters, which may result in excellent adhesion between nitrided layer and substrate.

The as-quenched microstructure of the present alloy is ductile γ phase containing an extremely high density of nano-sized κ′-carbides formed through spinodal decomposition during quenching. The as-quenched alloy is plasma-nitrided at 500 °C for 8 h, resulting in the effects of aging and nitriding simultaneously. Furthermore, the resultant 40 μm thick nitrided layer is composed predominantly of AlN, the nitrogen concentration at surface is extremely high up to 20 wt.%. Consequently, the surface microhardness (1860 Hv), substrate hardness (550 Hv), ductility (33.6%) and corrosion resistance in 3.5% NaCl solution of the present nitrided alloy are far superior to those obtained previously for the optimally nitrided high-strength alloy steels as well as martensitic and precipitation-hardening stainless steels.

Acknowledgements

This work was supported by the National Science Council, Taiwan (NSC-100-2221-E-009-053-MY3).

References

[1] G.S. Krivonogov, M.F. Alekseyenko, G.G. Solov'yeva, Fitz. Metal. Metalloved 9 (1975) 775.
[2] W.K. Choo, J.H. Kim, J.C. Yoon, Acta Mater. 45 (1997) 4877.
[3] I. Kalashnikov, O. Acselrad, A. Shalkevich, L.C. Pereira, J. Mater. Eng. Perform. 9 (2000) 597.
[4] Y.H. Tuan, C.S. Wang, C.Y. Tsai, C.G. Chao, T.F. Liu, Mater. Chem. Phys. 114 (2009) 595.
[5] M. Ruscak, T.P. Perng, Corrosion (October) (1995) 738.
[6] G.D. Tsay, Y.H. Tuan, C.L. Lin, C.G. Chao, T.F. Liu, Mater. Trans. 52 (2011) 521.
[7] K.M. Chang, C.G. Chao, T.F. Liu, Scripta Mater. 63 (2010) 162.
[8] Y. Li, L. Wang, D. Zhang, L. Shen, Appl. Surf. Sci. 256 (2010) 4149.
[9] T. Savisalo, D.B. Lewis, Q. Luo, M. Bolton, P. Hovsepian, Surf. Coat. Technol. 202 (2008) 1661.
[10] Y. Li, L. Wang, D. Zhang, L. Shen, J. Alloy Compd. 497 (2010) 285.
[11] P. Corengia, G. Ybarra, C. Moina, A. Cabo, E. Broitman, Surf. Coat. Technol. 187 (2004) 63.
[12] C.X. Li, T. Bell, Corros. Sci. 48 (2006) 2036.
[13] R.F. Liu, M.F. Yan, Mater. Des. 31 (2010) 2355.
[14] R.F. Liu, M.F. Yan, Surf. Coat. Technol. 204 (2010) 2251.
[15] W. Liang, Appl. Surf. Sci. 211 (2003) 308.
[16] L. Shen, L. Wang, Y. Wang, C. Wang, Surf. Coat. Technol. 204 (2010) 3222.
[17] C.X. Li, T. Bell, Corros. Sci. 46 (2004) 1527.
[18] H.R. Abedi, M. Salehi, Mater. Des. 32 (2011) 2100.
[19] M. Olzon-Dionysio, S.D. de Souza, R.L.O. Basso, S. de Souza, Surf. Coat. Technol. 202 (2008) 3607.
[20] S.H. Sheng, R.F. Zhang, S. Veprek, Acta Mater. 56 (2008) 968.
[21] Y. Utsushikawa, K. Niizuma, J. Alloy Compd. 222 (1995) 188.
[22] H.A. Wriedt, N.A. Gokcen, R.H. Nafziger, Bull. Alloy Phase Diagram 8 (1987) 355.
[23] W.P. Tong, N.R. Tao, Z.B. Wang, J. Lu, K. Lu, Science 299 (2003) 686.
[24] G.J. Li, J. Wang, Q. Peng, C. Li, Y. Wang, B.L. Shen, J. Mater. Proc. Technol. 207 (2008) 187.
[25] G.J. Li, J. Wang, C. Li, Q. Peng, J. Gao, B.L. Shen, Nucl. Instrum. Meth. B 266 (2008) 1964.
[26] J.K. Park, Y.J. Baik, Mater. Lett. 62 (2008) 2528.
[27] E.A. Ochoa, C.A. Figueroa, F. Alvarez, Surf. Coat. Technol. 200 (2005) 2165.
[28] Cubberly, W.H., Masseria, V., Kirkpatrick, C.W. and Sanders B. Metals Handbook, ninth ed., Heat Treating, vol. 4, American Society for Metals, Metals Park, OH, 1982.
[29] A. Neville, T. Hodgkiess, Corros. Sci. 38 (1996) 927.